Assessment of Motion Devices Used for Spatial Orientation Research and Training

Curtis H. Spenny and Bradley S. Liebst
Air Force Institute of Technology
Department of Aeronautics and Astronautics
2950 P Street, AFIT/ENY
Wright Patterson AFB, OH 45433-7769, USA

Phone: (937) 255-6565, x4320
Fax:(937) 656-7621
email: curtis.spenny@afit.edu

Summary

There are many unresolved issues related to motion-based simulators including: 1) should they even be used, 2) if so, what drive configurations might be preferred and to what aspects of flight should they be applied, 3) what motion cues and artifacts are critical, 4) what drive algorithm or set of drive algorithms best utilizes the motion capabilities of a given configuration to emulate critical aircraft motion cues while producing minimal artifacts, and 5) how can pilot-driven algorithms be made more effective at teaching recovery from the perceptual conflicts of spatial disorientation? None of these questions are answered by this paper. What the paper does contain is a description of the capability of a computer simulation of motion simulators that can be used to help quantitatively address these questions. A sample aircraft maneuver is evaluated for several variants of drive configuration and drive algorithm to illustrate the measures for quantitative comparison of motion systems and the level of effort and input data required to make the comparison. The paper indicates the status of an ongoing effort to develop a modeling tool for use by the spatial orientation and flight simulation communities to gain further understanding of the role of motion simulators.

1 INTRODUCTION

A fundamental characteristic of flight simulators is that changes in the visual out-the-window scene and instrument readings are pilot-driven in response to pilot sensory information obtained from those same visuals. Only commercial aviation makes significant use of motion simulators where the motion is part of the pilot-driven, pilot-sensed loop. The nature and relevance of motion cuing to general pilot proficiency is not well understood [1], although there are situations such as recovery from the sensory conflicts of illusion-producing motions where the motion requirements of the simulator are clearly understood and the presence of motion in the pilot-driven, pilot sensed loop is critical [3]. Assessment of the value of motion cues to general pilot proficiency has been investigated with mixed results. A US DOT study found the incremental value of motion to be immeasurable [4]. Others have concluded that prior experience with motion-based simulators was destined to fail, since the technologies applied to accomplish motion and synchronize it with visual cues has been very poor compared to present day capability [6]. In the case of the U.S. Air Force, fixed base is the simulator form used for both heavy and tactical classes of aircraft.

An important attribute of a motion-based flight simulator is rapid response to pilot input. The only perceived delay should be that of the particular aircraft flight control system being simulated. Any delay in response of the motion system must be recognized as 'un-airplane-like' and reduced to the smallest value possible. Further, synchronization between the visual and motion system responses must be minimized to

Paper presented at the RTO HFM Symposium on "Spatial Disorientation in Military Vehicles: Causes, Consequences and Cures", held in La Coruña, Spain, 15-17 April 2002, and published in RTO-MP-086.

avoid the possibilities of simulator sickness and negative training. These response traits can be evaluated via simulation or test by comparing the visual and motion response of the simulator with the aircraft motion that drives the simulation. Motion system delay via simulation was considered in reference [9] for a high g-trainer controlled to operate as a flight simulator. Evaluation of motion system delay via simulation requires an integrated model of the simulator dynamic system, including its motors and feedback control system and a predictor of human perception of motion.

A more fundamental issue with motion-based simulators is the degree to which an ideal motion-producing device, one with no time delay, can produce perceived motion in the rider that is similar to that perceived in an aircraft while not producing any deleterious motion artifacts. It can be categorically stated that no practical ground-based motion system can reproduce all motions that an aircraft is capable of producing since the simulator remains attached to the ground. Likewise, a ground-based motion system cannot emulate any aircraft motion except steady flight without creating some motion artifact. The drive mechanism used almost exclusively in motion simulators, is the Stewart platform. The philosophy of this drive algorithm is to provide acceleration onset cues that are 'airplane-like' followed by sub-threshold return of the actuators to their neutral position. The virtue of the Stewart platform is the ability to provide the onset of *any* aircraft transient motion. Its deficit is the inability to produce high and sustained g levels of aircraft, particularly tactical and aerobatic aircraft. Further, each return to sub-threshold acceleration level is a motion artifact. Drive mechanisms that have actuators configured in a series or cascade arrangement have been used to produce the sustained g-levels and sustained angular rates experienced in flight. They have found application for simulating specific maneuvers such as spatial illusions [5] and super-maneuvers that make use of thrust vectoring [7][11]. However, any particular configuration of a cascade device appears to be best suited to specific maneuvers, making it difficult to provide general simulator capability with a single device. Further, artifacts are always created by the arm rotation used to produce continuous acceleration or angular rate. While a fixed base simulator has no artifacts, it also has no motion cues. Thus, no motion (or no-motion) alternative is clearly superior. It seems appropriate to reexamine the statement "no motion is better than bad motion" in light of these observations and the recognition of improvements in motion control that are now available. The unresolved issue in attempting to incorporate the advantages of motion into flight simulators is not whether a Stewart platform or a centrifugal arm is best suited, but whether a high fidelity motion simulator can be developed that can accomplish the essential transient and continuous motion cues of flight with acceptably inconsequential artifacts.

This paper reports the progress of an ongoing study to investigate the capability to provide both *transient and continuous* motion cues to a pilot-driven simulator. To find an effective means to do so for any maneuver of any aircraft would markedly expand simulator usefulness for training to maintain spatial orientation and recover from spatial disorientation and for pilot training in general. But this is perhaps more than can be expected. To find a better means to do so only for selected maneuvers such as those that create vestibular illusions would provide a lesser but still significant expansion of simulator usefulness and, perhaps more importantly, help to clarify the role of motion in pilot training. Conclusions in this study are based on the output of a model of the vestibular end organ that attempts to predict perceived motion. Verification of conclusions must be obtained by subject testing in a prototype device.

2 Drive Mechanism Configurations

How many degrees of freedom (DoF) should a motion-based simulator possess? Since an aircraft possesses six degrees of freedom, three translational and three angular, intuitively it would seem that the drive should also contain six DoF. Such is the case for the Stewart platform. It consists of six prismatic (linear) actuators configured to act in parallel on the platform that, for flight simulator, is a replica of an aircraft cockpit. Because it possesses six DoF, it can duplicate the onset of all short duration motions of flight. It is, however, limited by stroke of the prismatic joints to providing onset cues for longer duration motions and accelerations. The Stewart platform is particularly suited to replicating the transients of helicopter motion and has found significant application in large transport aircraft and commercial airliners.

The other significant class of platforms used to produce motion in flight simulators is the cascade configuration which consists of revolute and prismatic joints configured in serial link or chain fashion with the cockpit attached at the end of the last link. Such cascaded devices can provide transient and continuous angular rates, transient and continuous linear accelerations at elevated levels, and transient angular accelerations all of which are present in the flight of high speed aircraft. Cascade mechanisms have been used predominantly to demonstrate spatial disorientation. They typically have three or four actuated joints which preclude simultaneous control of more than that number of degrees of platform freedom. The rationale for limiting control capability apparently is that some cues cannot be justified economically.

Table 1 summarizes the basic kinematic structure of illustrative motion-based devices built for use in flight simulators, where ***R*** and ***P*** designate revolute and prismatic joints, respectively. Kinematic configuration is not fully specified by kinematic structure. In addition to joint arrangement and type, the relative orientations of their axes of motion and the distance between joints are critical design variables that can affect the ability to duplicate a specific aircraft motion. In this study, a particular 3 DoF R-R-R cascade configuration, hereafter referred to as the 3R cascade drive, was selected for investigation that can be tailored to represent the DES, the IPT and certain 3 DoF motions performed by the ASDT. The relative orientation and distance between the three axes is depicted in Figure 1 for the device at rest. The parameters that can be varied are length L_2 of the planetary arm and distance L_3 of the vestibular point above or below the yoke point (YP) where second and third axes intersect. Three coordinate frames are indicated in Figure 1:

Frame 0 - Base Frame The zero frame is fixed to the earth with its origin, O_0, on the planetary axis and at the same elevation as the YP. z_0 is the axis of (vertical) planetary rotation and the angle swept out by the planetary arm is q_1. Note that the angular velocity is positive for clockwise rotation as seen from above (the DES rotates clockwise). When q_1 is a multiple of $2\pi, x_0$ is pointed along the arm towards YP. y_0 forms a right hand orthogonal coordinate set.

Frame v - Vehicle Frame Frame v is attached to the cab with its origin, O_v at the vestibular point. Axes are defined as conventional aircraft axes: x_v points in the forward facing direction of the pilot and is his roll axis, y_v points rightward along the pilot's pitch axis and z_v points downward along the pilot's yaw axis.

Device	# DoF	Joint Arrangement, Type	Owner or Mfr.
Dynamic Environment Simulator (DES)	3	Serial, R-R-R	WPAFB
GFET	3	Serial, R-R-R	ETC
IPT	4	Hybrid Serial/Parallel, R-P-R-R	ETC
Advanced Spatial Disorientation Trainer	4	Serial, R-R-R-R	Brooks AFB
Level C Flight Simulator	6	Parallel, P-P-P-P-P-P	FAA
Desdemona	6	Serial, P-P-P-R-R-R	AMST Corp

Table 1: Tabulation of the basic kinematic structure of illustrative motion-based simulators.

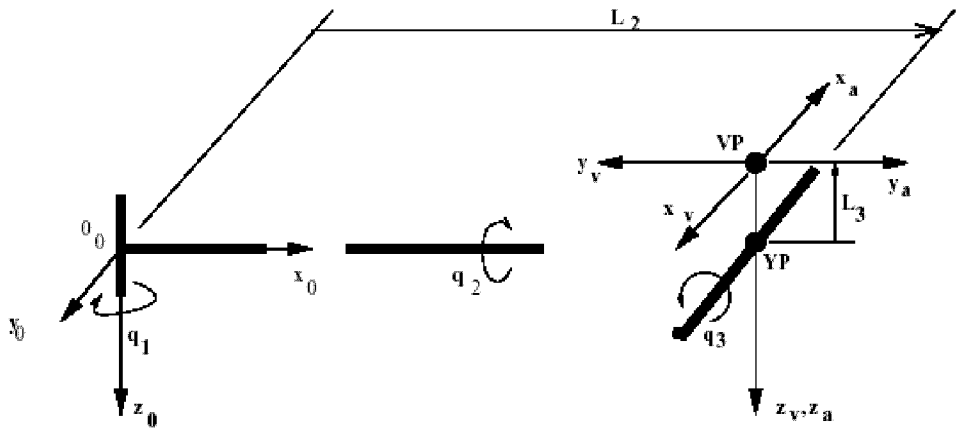

Figure 1: Coordinate frame definitions for the 3 DoF cascade drive configuration implemented in the kinematic model (shown at rest).

Frame a - Anatomical Frame Frame *a* is attached to the cab with its origin, O_a coincident with O_v. Axes are defined in anatomical directions: x_a points in the rearward facing direction of the pilot y_a points leftward with respect to the pilot and z_a points downward. Frame *a* is fixed with respect to frame *v* since no head motion is assumed.

In Figure 1, the rider is shown facing tangent to the path of the VP and in the forward direction for clockwise rotation of the planetary arm. Other rider orientations can also be specified in the input file for the simulation. Frame-*v* is used to express the state vectors in conventional aircraft components. Frame-*a* is used to express vectors in conventional anatomical components. The three joint variables $[q_1, q_2, q_3]$ define device position. It is noted in Figure 1 that for the centrifuge at rest, $q_1 = q_2 = \pi/2$ whereas $q_3 = 0$.

3 Model Description

How the number, type, orientation and spacing of the actuated joints influence the ability of a particular configuration to provide the requisite motion sensations and only non-deleterious artifacts can be quantified by modeling the *drive algorithm* that converts desired aircraft accelerations into commands to the joints of the drive mechanism and the *forward kinematics equation* of the drive mechanism that convert the joint commands into equivalent platform accelerations. If the drive algorithm were the mathematical inverse of the forward kinematics equations, the platform accelerations would precisely match the desired aircraft accelerations, the simulator would be precise at reproducing aircraft motion and there would be no motion artifacts. Because it is not the inverse for any practical drive mechanisms, this kinematic model is a useful tool for quantitatively comparing the performance of various drive algorithms and drive mechanism configurations. By consciously excluding from the model, the dynamic effects of the drive and motor and the delay of the feedback control strategy implemented, configuration alternatives can be more objectively evaluated and with a much reduced set of device characteristics.

Figure 2 identifies the eight Matlab modules that comprise the kinematic model used for this study. Input to the model, module 'Sensed Acceleration Input', is the sensed acceleration profile (including gravity) in the aircraft at the pilot vestibular point. The module 'Controller Commands' contains the drive algorithm. The forward kinematic equations are contained in the 'Output Processor' module. The forward kinematics portion of the model can be viewed as the plant or physical device and the drive algorithm as a command that drives the plant. There is one forward kinematic equation associated with a particular kinematic

configuration. There may be multiple drive algorithms associated with it. No other aspects of the motion simulator are included in the kinematic model. The modular structure minimizes the change out required to evaluate different simulators. Primary output data from the model is the level of DFS fidelity attainable and the magnitude of artifacts. Young's model of the vestibular end organ [12][13][14] is implemented in the module 'Vestibular Model' to evaluate the effects of accommodation and sub-threshold signals on perceived motion. The module 'Vestibular Model' also contains a scalar metric for measuring the fidelity of a maneuver that is the integral over the maneuver time of the root-sum-square of the normalized errors in each of the six acceleration components. The other modules, that are less relevant to the topic of this paper, are described briefly in figure 2.

The model was implemented with MATLAB™ and SIMULINK™ software.* The kinematic model becomes a dynamic model when the module "Ideal Plant Dynamics' is replaced by a model of the plant, drive motors and feedback controller for a particular motion simulator. The dynamic model of the GFET Tactical Flight Simulator is described in reference [9].

3.1 Sample Maneuver

A simple maneuver is used here to illustrate use of the model in evaluating the fidelity of a motion simulator. It is transition from steady level flight into a coordinated steady turn with a constant climb or descent, which can develop analytically. As will be illustrated, it is not a trivial maneuver to accomplish with fidelity by the motion drives investigated herein.

The aircraft is assumed to transition from steady, wings level flight to a steady, climbing (or descending) turn with bank angle $\phi(t)$ prescribed as a function of time. The transition is flown in such a way that the turn is coordinated at any instant. Following the kinematic definitions of Etkin [2], the orientation of an aircraft relative to an earth fixed frame is given by three Euler angles, $[\psi,\theta,\phi]$, a set of sequential rotations about axes *z*, then *y* and then *x* of the aircraft body frame (frame-*v* in this document). The associated Euler angular rates, $[\dot{\psi},\dot{\theta},\dot{\phi}]$, are related to the body rates, [*p,q,r*] by the equations:

$$\begin{aligned}\dot{\psi} &= (q\sin\phi + r\cos\phi)\sec\theta \\ \dot{\theta} &= q\cos\phi - r\sin\phi \\ \dot{\phi} &= p + (q\sin\phi + r\cos\phi)\tan\theta\end{aligned} \qquad (1)$$

* MATLAB and SIMULINK are registered trademarks of Mathworks, Inc., Natick, MA

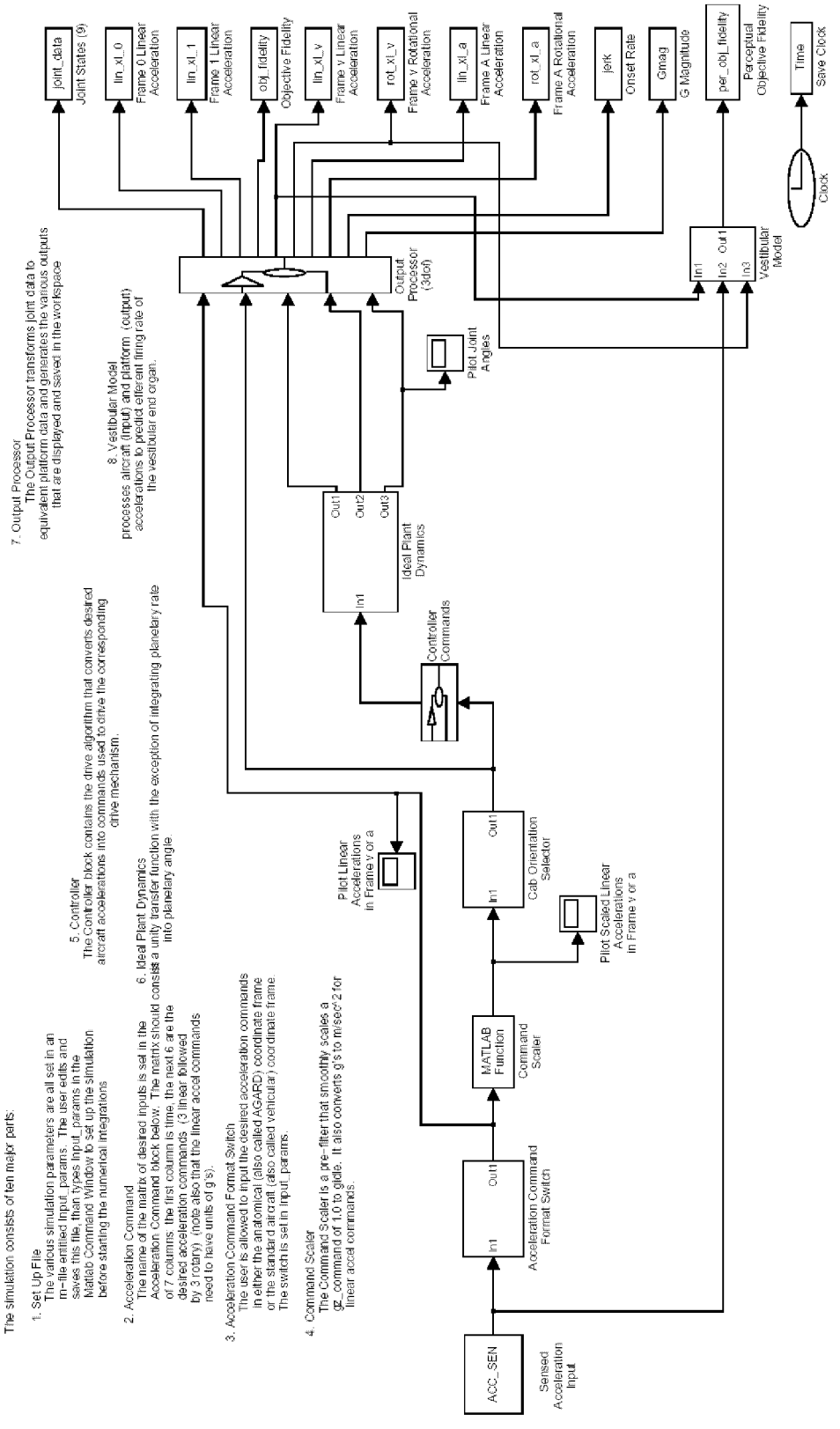

Figure 2: Simulink module representation of the kinematic model for motion simulator drives.

The g-level n, equation 2, turn rate $\dot{\psi}$, equation 3 and turn radius R, equation 4 that describe aircraft motion in a coordinated turn are also adapted from Etkin [2]:

$$n = \sec\phi \tag{2}$$

$$\dot{\psi} = \frac{g}{V}\tan\phi \tag{3}$$

$$R = V^2/(g\tan\phi) \tag{4}$$

where g is the acceleration of gravity and V is aircraft speed. Then, the frame-v components of the acceleration commands at the aircraft center of mass are given by:

$$\begin{Bmatrix} G_x \\ G_y \\ G_z \\ \alpha_x \\ \alpha_y \\ \alpha_z \end{Bmatrix}_v = \begin{Bmatrix} 0 \\ 0 \\ -n(t) \\ \dot{p}(t) \\ \dot{q}(t) \\ \dot{r}(t) \end{Bmatrix}_v \tag{5}$$

where G_i is the i^{th} component of sensed rectilinear acceleration normalized by g, α_i is the i^{th} component of angular acceleration, and 'sensed' is used here to mean inclusion of gravity. Alternatively, when the pilot vestibular location is displaced from the aircraft center of mass by a distance $[r_x, r_z]$, the resulting profile is given by:

$$\begin{Bmatrix} G_x \\ G_y \\ G_z \\ \alpha_x \\ \alpha_y \\ \alpha_z \end{Bmatrix} = \begin{Bmatrix} \left(r_x\left(r^2 - q^2\right) - r_z rp + \dot{q}r_z\right)/g \\ \left(r_x pq + r_z qr + \dot{r}r_x - \dot{p}r_z\right)/g \\ -n(t) + \left(r_x rp - r_z\left(q^2 + p^2\right) - \dot{q}r_x\right)/g \\ \dot{p}(t) \\ \dot{q}(t) \\ \dot{r}(t) \end{Bmatrix} 1/g \tag{6}$$

where n is given as a function of ϕ by equation 2 and the body rates [p, q, r] and their derivatives can be determined as a function of ϕ using equations 1. The assumed bank angle ϕ for three phases of the maneuver are:

Steady, level flight, $t < T_s$:

$$\phi(t) = 0 \tag{7}$$

Transition, $T_s < t < T_f$:

$$\phi(t) = \frac{\phi_f}{2}(1 - \cos\omega t) \tag{8}$$

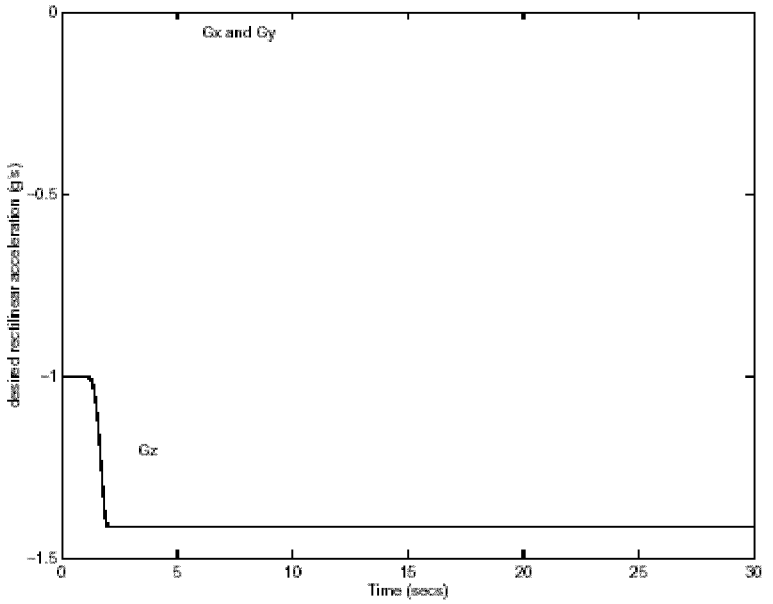

Figure 3: G_x, G_y, G_z sensed accelerations for the sample maneuver with $r_x = r_z = 0$.

Steady coordinated turn, $t > T_f$:

$$\phi(t) = \phi_f \tag{9}$$

where T_s and T_f are the start and finish times of the transition from steady level flight to a steady coordinated turn.

Equations 5 are evaluated for transition to a $\sqrt{2}g$ turn in 1 second starting after 1 second of level flight and produce linear and angular acceleration commands as indicated in figures 3 and 4, respectively. The large spikes in α_x result from the step change in prescribed roll acceleration $\ddot{\phi}$ at the start and end of the transition. In figure 5, where the vestibular point is located 3m forward $(r_x = 3m)$ and 0.5m above the center of mass $(r_z = -0.5m)$, there is a large spike in G_y, as well, produced by the roll acceleration for the same transition.

3.2 Forward Kinematic Equations

The equation that relates frame *v* components of sensed acceleration to the plant joint states for the 3DoF revolute drive of figure 1 is:

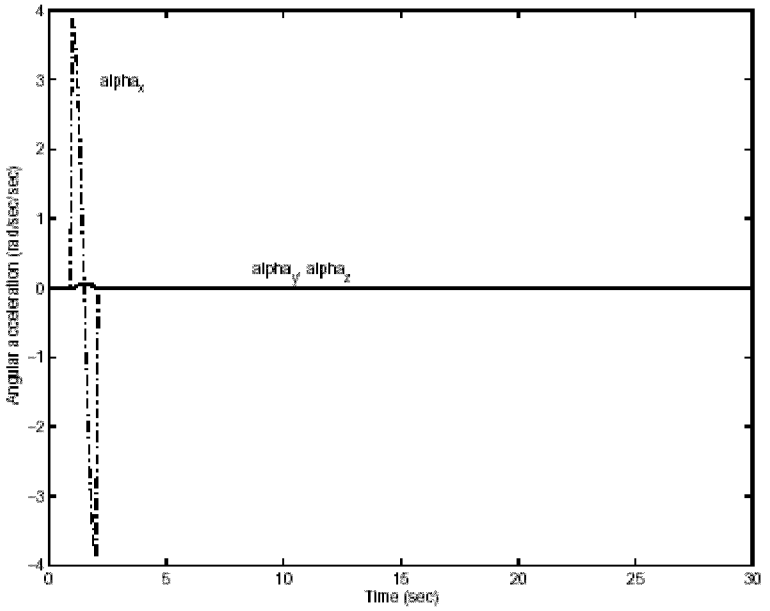

Figure 4: Angular accelerations for the sample maneuver.

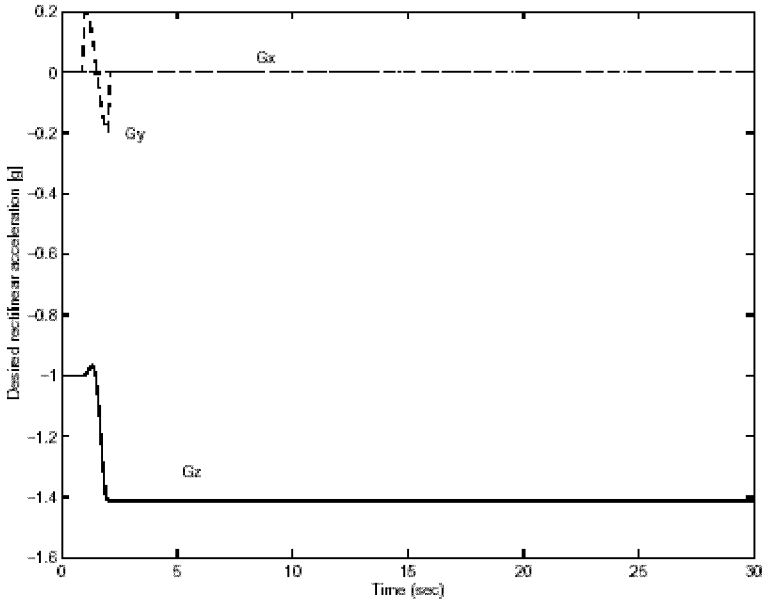

Figure 5: G_x, G_y, G_z sensed accelerations for the sample maneuver with $r_x = 3m$ and $r_z = -0.5m$.

$$\begin{Bmatrix} \ddot{x}_s \\ \ddot{y}_s \\ \ddot{z}_s \\ \cdot\cdot \\ \alpha_x \\ \alpha_y \\ \alpha_z \end{Bmatrix}_v = J_v \begin{Bmatrix} \ddot{q}_1 \\ \ddot{q}_2 \\ \ddot{q}_3 \end{Bmatrix} + \left[\dot{J}_v\right] \begin{Bmatrix} \dot{q}_1 \\ \dot{q}_2 \\ \dot{q}_3 \end{Bmatrix} - g \begin{Bmatrix} C_2 \\ S_2 S_3 \\ C_3 S_2 \\ \cdots\cdots \\ 0 \\ 0 \\ 0 \end{Bmatrix} \tag{10}$$

where $[\ddot{x}_s, \ddot{y}_s, \ddot{z}_s]$ are the rectilinear components of sensed acceleration (not normalized), S_i and C_i are the sine and cosine of joint variable q_i, the single and double dots over joint variables indicate their first and second derivatives, respectively, J_v is given by

$$J_v = \begin{bmatrix} -S_2(L_2 + L_3 S_3) & -L_3 C_3 & 0 \\ C_2(L_3 + L_2 S_3) & 0 & L_3 \\ L_2 C_2 C_3 & 0 & 0 \\ \cdots\cdots\cdots\cdots\cdots & \cdots\cdots\cdots & \cdots \\ C_2 & 0 & 1 \\ S_2 S_3 & C_3 & 0 \\ C_3 S_2 & -S_3 & 0 \end{bmatrix} \tag{11}$$

and $\dot{J}_v$ is given by

$$\begin{bmatrix} -L_3 C_3 S_2 (C_2 \dot{q}_1 + \dot{q}_3) & L_3 S_3 \dot{q}_3 & L_3 (S_3 \dot{q}_2 - C_3 S_2 \dot{q}_1) \\ -C_3 \left(L_2 + L_3 S_2^2 S_3\right) \dot{q}_1 - L_3 C_3^2 S_2 \dot{q}_2 & L_3 C_3 (S_3 \dot{q}_2 - C_3 S_2 \dot{q}_1) & 0 \\ \left(L_3 \left(3 + C_{2q2} - 2C_{2q3} S_2^2\right) + 4 L_2 S_3\right) \dot{q}_1 / 4 & L_3 C_3 (S_2 S_3 \dot{q}_1 + C_3 \dot{q}_2) & L_3 C_2 \dot{q}_1 + \dot{q}_3 \\ + 2 L_3 \left(S_2 S_{2q3} q_2 + 2 C_2 q_3\right) / 4 & & \\ \cdots\cdots\cdots\cdots\cdots\cdots\cdots\cdots\cdots & \cdots\cdots\cdots\cdots\cdots\cdots & \cdots\cdots\cdots\cdots\cdots \\ 0 & -S_2 \dot{q}_1 & 0 \\ 0 & C_2 S_3 \dot{q}_1 & C_3 S_2 \dot{q}_1 - S_3 \dot{q}_2 \\ 0 & C_2 C_3 \dot{q}_1 & -S_2 S_3 \dot{q}_1 - C_3 \dot{q}_2 \end{bmatrix} \tag{12}$$

It can be observed in equation 10 that precise duplication of all six components of aircraft acceleration is possible only when simulating an aircraft in steady state. To illustrate, if $\dot{q}_1 = const.$, $q_2 = const.$ and $q_3 = const.$, the three components of aircraft rectilinear acceleration, $\ddot{x}_s, \ddot{y}_s$ and $\ddot{z}_s$ can be maintained at constant, non-zero values and the aircraft angular accelerations α_x, α_y and α_z are zero as required for steady flight. However, if the drive must be accelerated to change the aircraft rectilinear accelerations as a function of time in a specified way, then drive angular accelerations $\ddot{q}_1, \ddot{q}_2$ and $\ddot{q}_3$ must be specified as a function of time. As a result, the aircraft angular acceleration values are also specified as a function of time and, hence, will not match the desired aircraft angular acceleration profiles. Aircraft maneuvers that include variable levels of acceleration, such as transition between steady flight conditions, are the source of artifacts in motion simulators with revolute joints.

The forward kinematic equation 10 is embedded in the 'Output Processor' module of figure 2. It is valid for all of the motion type devices considered in this paper. Note for example a 1*g*-cascaded drive is modeled by setting $L_2 = 0$, a > 1*g*-cascaded drive by setting L_2 equal to planetary arm length. In general, the forward kinematic equation differs for each drive configuration. The forward kinematic equation can be generated symbolically for any cascade device using model development procedures for robotic devices [10] and the Mathematica™ software.*

3.3 Selected Drive Algorithms

A range drive algorithms can be devised for a particular drive configuration with the goal of providing fidelity of selected critical motion cues of a particular aircraft maneuver while also creating minimal artifacts. Three drive algorithms are presented here that provide different sets of critical cues, applicable for the 3R cascade configuration. Input to each is instantaneous aircraft data that makes the algorithm suitable for a pilot-driven simulator. In cases I and III where the moment arm L_2 is finite in length, the platform is assumed to be facing tangent to its trajectory about joint 1.

3.3.1 Case I: Drive Algorithm for Otolithic Critical Perception

While there are six independent components of vestibular acceleration experienced by an aircraft pilot, there are only three joint variables available to produce a desired response for the 3DoF-cascaded simulator. Thus, all vestibular components cannot be simultaneously controlled to their desired values. In this section, control of the linear acceleration components is formulated as the command for driving the motion system. This permits the motion system to control the magnitude and orientation of the sensed g-vector relative to the simulator to be that experienced in an aircraft with the desired acceleration profile. Thus, the otoliths of the rider of the simulator are exposed to the appropriate motion cues.

Joint commands q_i are related to the aircraft (frame-*v*) linear accelerations by solving the upper partition of equation 10 for joint angular accelerations in terms of the frame-*v* linear accelerations. L_3 is set to a nominal value of zero in solving since it is desirable to limit the nonlinear coupling between components of commanded joint acceleration. Note the upper partition of the matrix J_v defined by equation 10 is mathematically singular for this assumption. Thus, the matrix cannot be inverted and the physical interpretation is that there is no way to directly control all three components of a/c linear acceleration with this kinematic configuration. An inverse solution can be *devised* that has the desired effect.

Planetary Commands - The sensed acceleration level a_{mag} can be determined by taking the magnitude of upper partition of equation 10:

$$\begin{aligned} a_{mag} &= \sqrt{\ddot{x}_S^2 + \ddot{y}_S^2 + \ddot{z}_S^2} \\ &= \sqrt{\left(-L_2\dot{q}_1^2\right)^2 + \left(-g\right)^2 + \left(L_2\ddot{q}_1\right)^2} \end{aligned} \tag{13}$$

Equation 13 is frequently referred to as the centrifuge characteristic equation [8]. It is a highly nonlinear differential equation that relates the joint space variable $\dot{q}_1$ to task space (i.e. frame *v*) variable a_{mag}. It (presumably) cannot be solved analytically. Further, numerical solution must be accomplished in two parts depending on whether the centrifuge is accelerating or decelerating. A useful drive algorithm for the first

* Mathmatica is a registered trademark of Wolfram Research, Inc., Champaign, IL

joint (the planetary arm speed) can be established by setting $\ddot{q}_1 = 0$ in the characteristic equation in order to determine a commanded angular rate $\dot{q}_1^{com}$:

$$\dot{q}_1^{com} \approx \sqrt[4]{\left(a_{mag} / L_2\right)^2 - \left(g / L_2\right)^2} \tag{14}$$

Platform Orientation Commands - The second row of equation 10 can be solved for the 'command' joint angle q_2^{com} and is given by

$$q_i^{com} = \arcsin\left\{-b/2a \pm \sqrt{(b/2a)^2 - c/a}\right\} \tag{15}$$

where $i = 2$, $a = L_2^2\left(\ddot{q}_1^{com}\right)^2 + g^2, b = 2\ddot{x}_s^{des} L_2 \ddot{q}_1^{com}$ and $c = \left(\ddot{x}_s^{des}\right)^2 - g^2$. Since q_2 is always positive, the positive root from the quadratic is used.

The third row of equation 10 can be solved for the 'command' joint angle q_3^{com} and is given by equation 15 where $i = 3$, $a = L_2^2\left(\dot{q}_1^{com}\right)^4 + g^2 \sin^2 q_2^{com}, b = \left(\ddot{y}_s^{des} - L_2 \ddot{q}_1^{com} \cos q_2^{com}\right) 2g \sin q_2^{com}$ and $c = \left(\ddot{y}_s^{des} - L_2 \ddot{q}_1^{com} \cos q_2^{com}\right)^2 - L_2^2\left(\dot{q}_1^{com}\right)^4$. For the computation of q_3, the sign of the radical in equation 15 is determined by the sign of $\ddot{q}_1^{com}$. Planetary angular acceleration $\ddot{q}_1$ appears in the equation and must be measured, estimated or omitted. Because platform pitch is strongly effected by planetary angular acceleration and it should not be omitted. It can be obtained by differentiating equation 14.

The drive algorithm presented above is that which drives the dynamic model of motion drives (not presented here). The dynamic model presumes that the platform motion is pilot-driven and hence is configured to only accept instantaneous inputs that are available from a simulator's aircraft model. For the kinematic model of motion drives, additional knowledge of the aircraft maneuver is needed to produce the first and second derivatives of the joint variables, $[\dot{q}_1, \dot{q}_2]$ and $[\ddot{q}_1, \ddot{q}_2]$ that, for the dynamic model, are produced by the model in response the drive algorithm. These derivatives can be determined for analytical maneuvers such as the one presented in this paper by sequentially evaluating two differentiations of equation 15, their functional form being:

$$\dot{q}_2 = \dot{q}_2\left(\dot{q}_1, \ddot{q}_1, q_2\right) \tag{16}$$

$$\ddot{q}_2 = \ddot{q}_2\left(\dot{q}_1, \ddot{q}_1, q_1^{(3)}, q_2, \dot{q}_2\right) \tag{17}$$

$$\dot{q}_3 = \dot{q}_3\left(\dot{q}_1, \ddot{q}_1, q_1^{(3)}, q_2, \dot{q}_3\right) \tag{18}$$

$$\ddot{q}_3 = \ddot{q}_3\left(\dot{q}_1, \ddot{q}_1, q_1^{(3)}, q_1^{(4)}, q_2, \dot{q}_2, \ddot{q}_2, q_3, \dot{q}_3\right) \tag{19}$$

with derivatives of q_1 expressed in terms of $\ddot{z}$ and its higher derivatives, all of which can be expressed as a function of the assumed bank maneuver, ϕ.

3.3.2 Case II: Drive Algorithm for Semicircular Critical Perception

The lower partition of matrix J_v of equation 10 is not singular, which suggests it is possible to express device angular accelerations $\ddot{q}_1$ as function of aircraft angular accelerations. A drive algorithm can be constructed using this inverse that would be appropriate if it were desired to produce angular acceleration *onset* cues that matched those of the aircraft. The device would function similar to the Stewart platform in

that it would provide onset angular acceleration cues (but not rectilinear ones) that would precisely match those of the aircraft. There would be no angular artifacts. However, the magnitude and direction of the sensed g-vector would be dictated by the commands to achieve angular acceleration fidelity, thus failing to emulate the rectilinear accelerations of the aircraft and creating rectilinear artifacts. These artifacts are not present in the Stewart platform.

Another algorithm is presented here, that can be used to produce the *continuous* angular velocity cues that can lead to spatial disorientation by confusing the senses of the semicircular canals. For a bank maneuver, the rotary device (i.e. the 3 DoF cascade device with a planetary arm length of zero), the following commands produce reasonable yaw and roll fidelity:

$$\dot{q}_1^{com} = K_{SD}\dot{\psi} \tag{20}$$

$$q_2^{com} = \pi/2 \tag{21}$$

$$q_3^{com} = k_{cross}\phi \tag{22}$$

where K_{SD} and k_{cross} are constants that are used to tune the fidelity of the simulator. The maneuver variables on the right hand side of equations 20-22 can constructed from instantaneous output of a simulator's aircraft model, and, hence, can be used for a pilot-driven simulator. Since the drive algorithm does not utilize equation 15, derivatives of the joint variables in the kinematic model are computed directly from the maneuver variable ϕ.

3.3.3 Case III: Drive Algorithm for Mixed Otolith/Semicircular Critical Perception

It is possible to provide fidelity that is a combination of otolith and semicircular senses. The Case III objective is to provide elevated g-level cues in conjunction with high fidelity roll acceleration, using a drive with a finite length planetary arm L_2. Device joint (q_2) is locked in order to eliminate a pitch artifact, recognizing there will be a degradation in distribution of g-acceleration between components. It is a combination of Cases I and II:

$$\dot{q}_1^{com} \approx \sqrt[4]{(a_{mag}/L_2)^2 - (g/L_2)^2} \tag{23}$$

$$q_2^{com} = \pi/2 \tag{24}$$

$$q_3^{com} = q_{3init} + k_{cross}\phi \tag{25}$$

where q_{3init} is the initial roll orientation of the platform as determined for the selected idle speed.

4 Results and Discussion

The results are presented for each of the three drive algorithms defined in the previous section, by comparing plots of the time history of selected components of aircraft acceleration with the corresponding motion system output. All of the drive algorithms are devised for the same kinematic configuration, the 3R cascade, and all results are for the same maneuver, transition into a coordinated turn. In all cases, the model starts with the aircraft flying straight-and-level. Initial conditions of the drive and the vestibular system are set to the corresponding steady state values. In cases I and III, the simulator is spinning at the start at a specified idle speed that increases the simulator g-level above 1g. In figure 6 the initial simulator acceleration of 1.28g can be observed. In case II where $L_2 = 0$, idle speed has been set to zero, as can be seen in figure 8. All data presented here is in frame-v components so z-direction acceleration for level flight is negative. The data is also computed is anatomical coordinates.

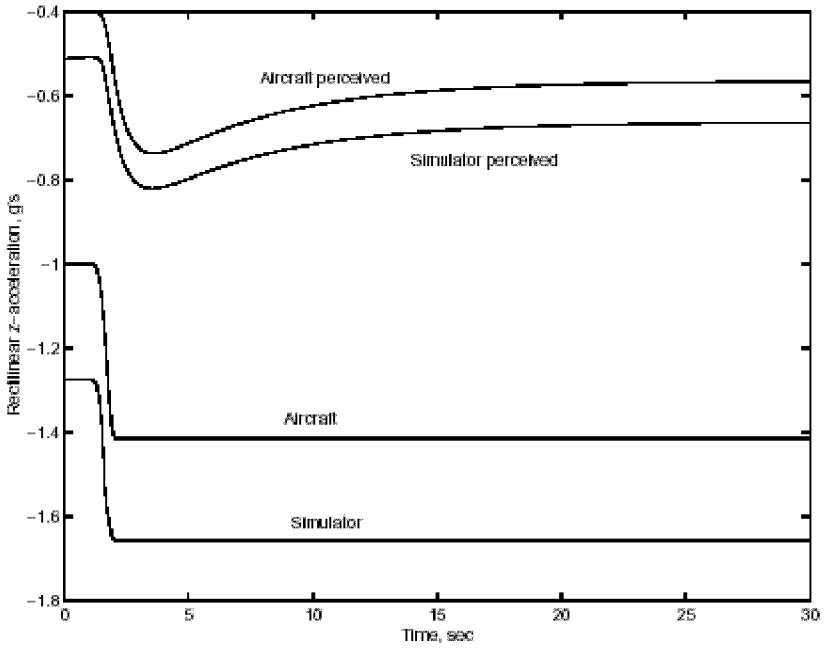

Figure 6: Comparison of aircraft and Case I simulator G_z acceleration for the sample maneuver.

In figure 6, the simulator acceleration is seen to have no delay in responding to the aircraft roll maneuver. This is because the kinematic model contains only the command to the drive, and excludes all of the dynamics of the motion system, motor delays and the error in the feedback control. Reference [9] describes a similar model configured with a dynamic module for analysis of response time. Also shown in figure 6 and several others that follow, is perceived motion as computed with a version of Young's vestibular model embedded in the kinematic model. Both the aircraft input and the simulator output are presented as perceived time histories. The perceived amplitude is 'efferent firing' level, so only relative amplitudes between perceived senses should be compared. The drop off in otolith perception in figure 6, when compared to the persistence of the actual simulator acceleration, G_z illustrates the accommodation characteristic of Young's model.

In figure 7, the simulator roll response is seen to have both magnitude and phase differences relative to the aircraft roll. The simulator roll response for the Case I algorithm, is that required to orient the platform so that the linear acceleration vector is entirely G_z. The delay in perceived response of the Semicircular canals is seen to be approximately 0.3 seconds.

Case II is shown in figures 8 to 11. Figures 8 and 9 are for the parameters $K_{SD} = 10$ and $k_{cross} = 0.5$. The simulator is seen to have roll response comparable in shape to that of the aircraft, but approximately one-half of the magnitude. The G_z acceleration becomes more positive (reduces) as the platform rolls, with G_y the component (not shown) becoming nonzero. This is the 'price' of attempting to attain roll fidelity with this device and this algorithm. Figures 10 and 11 shows that roll fidelity can be made precise by setting $k_{cross} = 1$, at the expense of even more loss in G_z fidelity.

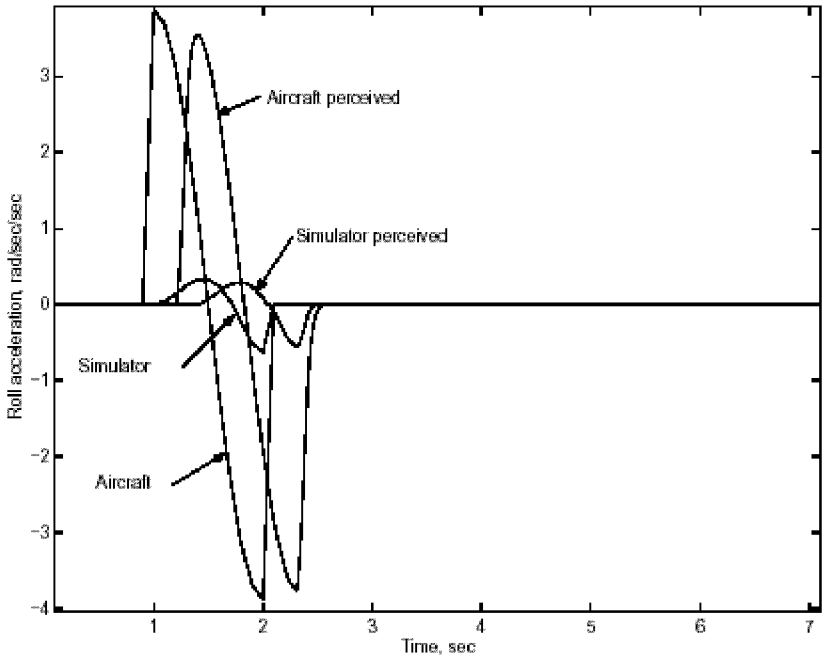

Figure 7: Comparison of aircraft and Case I simulator roll acceleration for the sample maneuver.

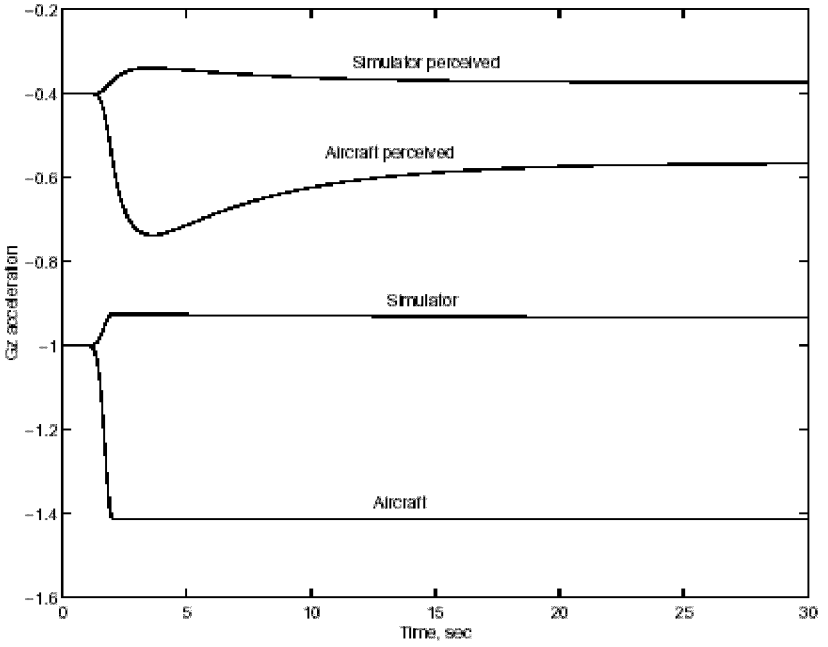

Figure 8: Comparison of aircraft and Case II simulator G_z acceleration for the sample maneuver with $k_{cross} = 0.5$.

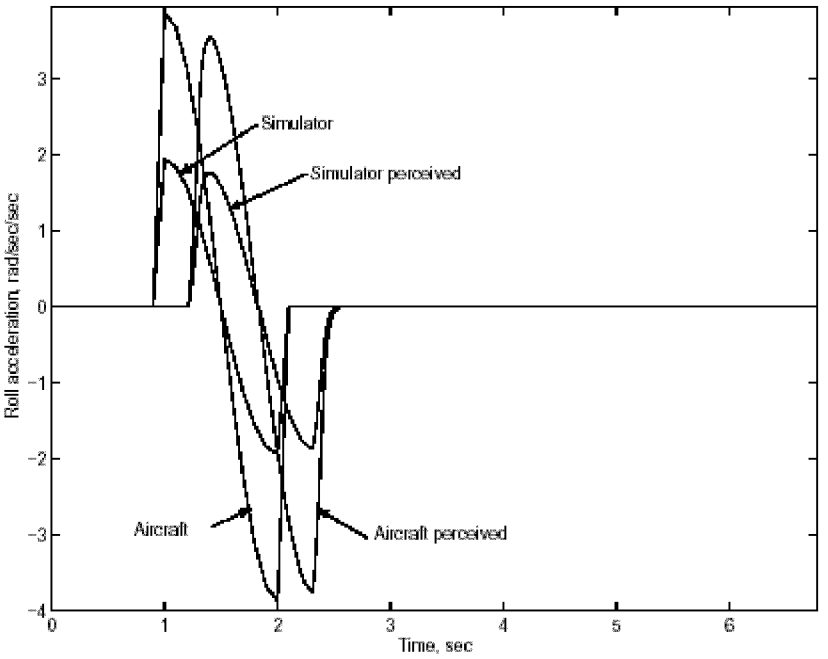

Figure 9: Comparison of aircraft and Case II simulator roll acceleration for the sample maneuver with $k_{cross} = 0.5$.

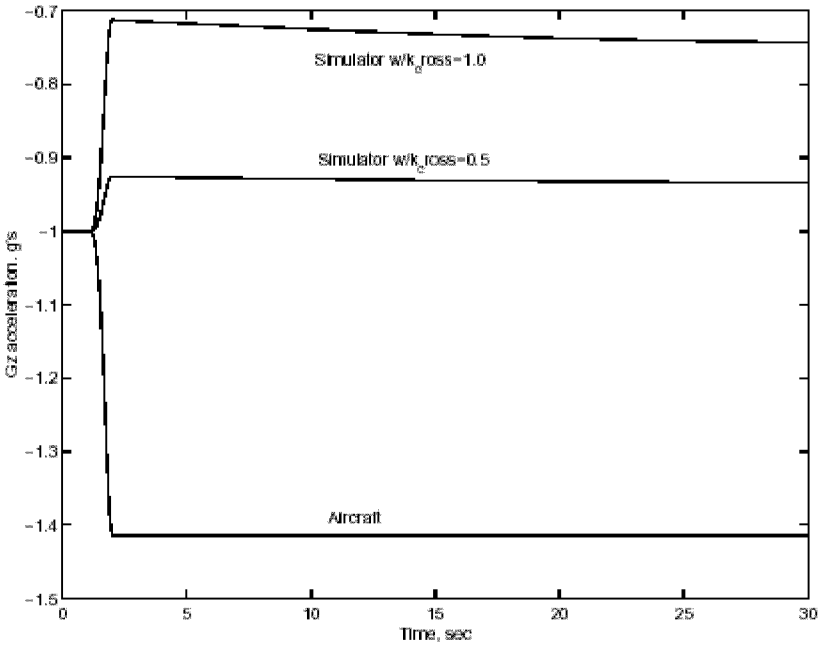

Figure 10: Comparison of aircraft and Case II simulator G_z acceleration for the sample maneuver with k_{cross} parameterized.

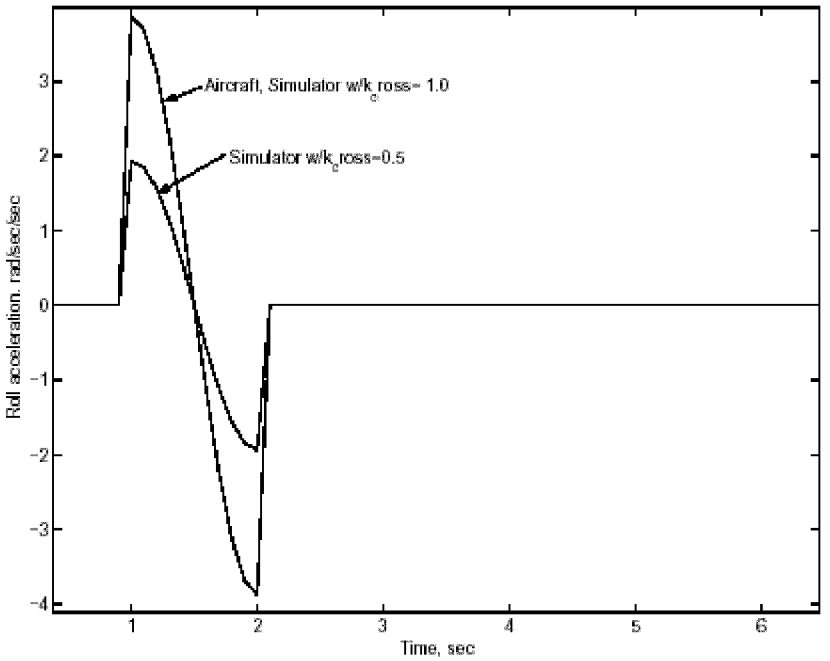

Figure 11: Comparison of aircraft and CASE II simulator roll acceleration for the sample maneuver with k_{cross} parameterized.

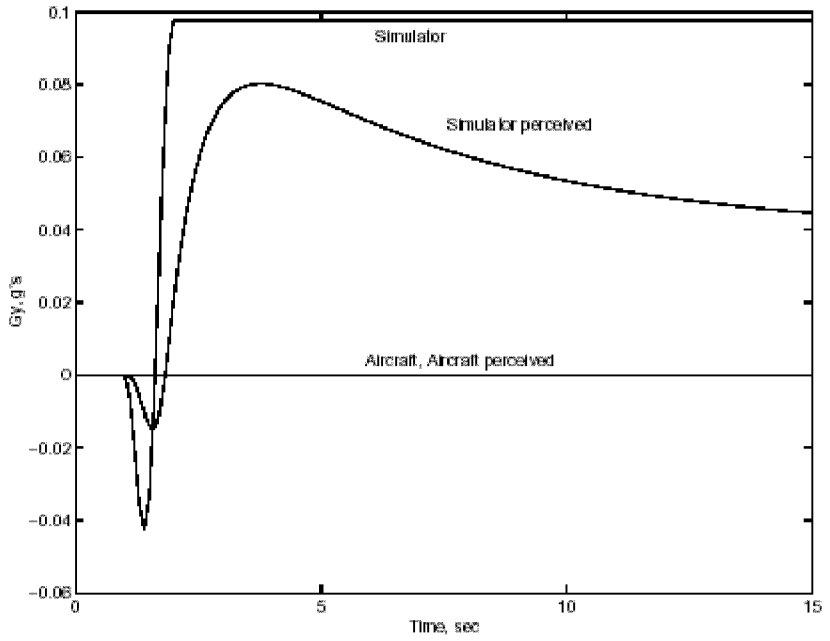

Figure 12: Comparison of aircraft and Case III simulator G_y acceleration for the sample maneuver.

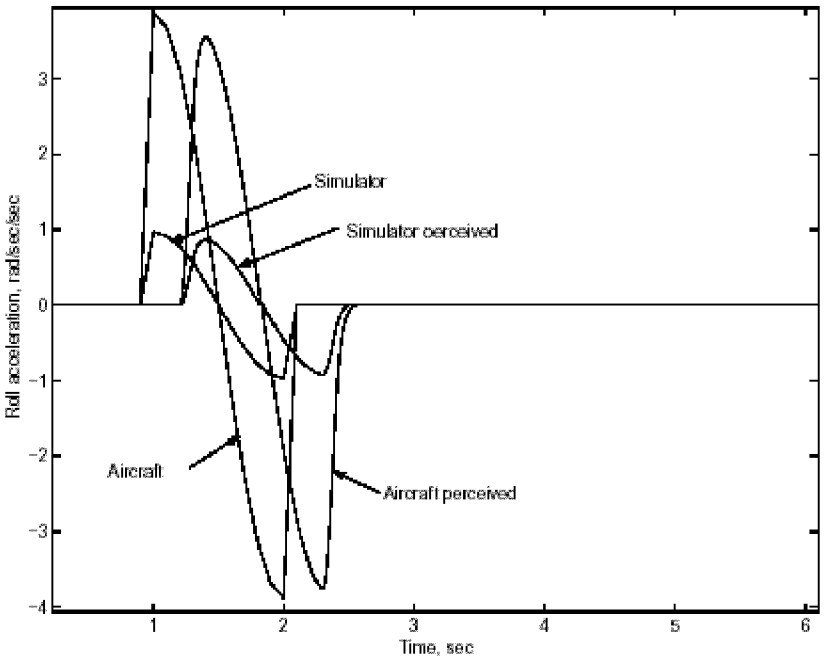

Figure 13: Comparison of aircraft and Case III simulator roll acceleration for the sample maneuver.

Case III is illustrated in figures 12 and 13 with $k_{cross} = 0.25$. The simulator is seen to have roll response comparable in shape to that of the aircraft, but approximately one-fourth of the magnitude. There is a $G_y \approx 0.1$ artifact created. G_z is comparable in shape and magnitude to that of figure 6.

It is noted that very little device specific data was required to obtain these comparative results. Depending on ones point of view, the performance of this R-R-R cascade drive and these drive algorithms might be considered adequate or appalling. None of the algorithms that have been compared here precisely match all aircraft accelerations. On the other hand, how much artifact is too much is not a well-defined. Recent tests by Chelette [9], for example, have shown that very high angular accelerations are perceived as only slightly disturbing. Further, the range of application of a device strongly influences how much artifact is produced. There are no motion simulators currently marketed that are capable of producing both transient and sustained 6 DoF response of full flight and there probably never will be since that would entail flying the simulator. There are, however, devices currently marketed that are highly capable for specific applications such as producing spatial illusions. An open question is whether additional aircraft response can be implemented in motion simulators that would enhance pilot training through economy and reduction in risk to life.

Options to be explored are: 1) identification of improved algorithms for existing drive configurations, 2) identification of new drive configurations and drive algorithms that would extend and improve on the capability of existing devices, and 3) identification of a highly redundant drive configuration and set of drive algorithms that could provide general purpose training, perhaps by changing algorithms 'on-the-fly' in response to flight conditions derived from the simulator's aircraft model. The kinematic/dynamic model being developed by the authors seems to be a useful tool for predicting the performance obtained these options as well as for other applications such as establishing quantitative requirements for motion simulators. The kinematic model requires minimal characterization of the drive device. The dynamic model requires a rather detailed set of drive system parameters. Both models would appear to be useful as design and assessment tools prior to the more costly and time consuming step of prototype development.

References

[1] Brown, Cardullo, McMillan, Riccio, and Sinacori, "New Approaches to Motion Cuing in Flight Simulators," Armstrong Laboratory, Air Force Material Command, September 1991.

[2] Etkin, Bernard, **Dynamics of Atmospheric Flight**, Wiley, 1972.

[3] Gillingham, Kent K., "Spatial Orientation in Flight," U.S. Air Force Technical Report AL-TR-1993-0022, Brooks AFB, TX, November 1993.

[4] Go, Tiauw H., J. Burki-Cohen and N. Soja, "The Effect of Simulator Motion on Pilot Training and Evaluation," Paper AIAA-2000-4296, Proceedings of the AIAA Modeling and Simulation Technologies Conference, Aug 2000.

[5] Leland, Dick, "Gyro IPT II "Second Generation Integrated Physiological Trainer," Environmental Tectonics Corporation, Southampton, PA 13 Oct 2000.

[6] Heintzman, Richard J., "Determination of Force Queing Requirements for Tactical Combat Training Devices, "Air Force Research Laboratory Contractor Rpt AFRL-TR-97-5001, Simtec, Inc., Manasas, VA February 1996.

[7] Repperger, D. W. and R.G. Roberts, "Aerospace robotics in supermaneuverable flight - defining the set of attainable motion fields in existing aircraft and motion simulators," Paper presented at the National Aerospace Electronics Conference (NAECON), Dayton, OH, May 1995.

[8] Smith et al, "A Mathematical Model for Centrifuge Simulators," Armstrong Laboratory, Air Force Material Command, December 1995.

[9] Spenny, C.H., B. Liebst, T. Chelette, C. Folescu, J. Sigda, "Development of a Sustainable-G Dynamic Flight Simulator," Paper AIAA 2000-4075, Proceedings of the AIAA Modeling and Simulation Technologies Conference, Denver, CO, Aug 2000.

[10] Spong M. and Vidyasagar M., **Robot Dynamics and Control**, Wiley, 1989

[11] van Poppi, Jon, B. Barton, D. Panncratz, M. Rangel, R. Banks, B.J. Bomar, "Simulation of Thrust Vectored Aircraft Maneuvers in a Human Centrifuge: Model Validation and Design for the Dynamic Environment Simulator," US Air Force Contractor Report AFRL-HE-WP-TR-1998-0138, Bomar Research Corporation, September 1998.

[12] Young, L.R., "The current status of vestibular systems models," Automatica, Vol. 5, pp 368-383, 1969.

[13] Young, L.R. and J.L. Meiry, "A revised dynamic otolith model," Aerospace Medicine Journal, pp 606-621, Jan 1968.

[14] Young, L.R. and C.M. Oman, "Model for vestibular adaptation to horizontal rotation," Aerospace Medicine, Vol 40, No. 10, pp 1076-1080, Oct 1969.